

A Free Web Service for Fast COVID-19 Classification of Chest X-Ray Images with Artificial Intelligence

Jose David Bermudez Castro[1(✉)], Jose E. Ruiz[1], Pedro Achanccaray Diaz[1], Smith Arauco Canchumuni[1], Cristian Muñoz Villalobos[1], Felipe Borges Coelho[1], Leonardo Forero Mendoza[2], and Marco Aurelio C. Pacheco[1]

[1] Pontifical Catholic University of Rio de Janeiro, Rua Marquês de São Vicente, 225, Gávea, Rio de Janeiro, RJ 22451-900, Brazil
prof.bermudez@ica.ele.puc-rio.br

[2] Rio de Janeiro State University, Block C - Floor 9, R. São Francisco Xavier, 524, Maracanã, Rio de Janeiro, RJ 20550-900, Brasil
https://www.puc-rio.br

Abstract. The coronavirus outbreak became a major concern for society worldwide. Technological innovation and ingenuity are essential to fight COVID-19 pandemic and bring us one step closer to overcome it. Researchers over the world are working actively to find available alternatives in different fields, such as the Healthcare System, pharmaceutic, health prevention, among others. With the rise of artificial intelligence (AI) in the last 10 years, IA-based applications have become the prevalent solution in different areas because of its higher capability, being now adopted to help combat against COVID-19. This work provides a fast detection system of COVID-19 characteristics in X-Ray images based on deep learning (DL) techniques. This system is available as a free web deployed service for fast patient classification, alleviating the high demand for standards method for COVID-19 diagnosis. It is constituted of two deep learning models, one to differentiate between X-Ray and non-X-Ray images based on Mobile-Net architecture, and another one to identify chest X-Ray images with characteristics of COVID-19 based on the DenseNet architecture. For real-time inference, it is provided a pair of dedicated GPUs, which reduce the computational time. The whole system can filter out non-chest X-Ray images, and detect whether the X-Ray presents characteristics of COVID-19, highlighting the most sensitive regions.

Keywords: COVID-19 · Deployed system · Free web service · Deep learning

© The Author(s), under exclusive license to Springer Nature Switzerland AG 2022
O. Gervasi et al. (Eds.): ICCSA 2022, LNCS 13375, pp. 412–427, 2022.
https://doi.org/10.1007/978-3-031-10522-7_29

1 Introduction

The coronavirus disease 2019 (COVID-19) was declared a public health emergency of international concern by the World Health Organization (WHO) on January 30 [1]. COVID-19 has become a pandemic with more than 120 million confirmed cases and almost 3 million deaths around 223 countries [2] at the time of writing this work. There have been many efforts to fight COVID-19 around the world such as research a vaccine against COVID-19, massive creation of ventilators as well as personal protective equipment (PPE), development of fast diagnosis systems from chest X-Ray and/or thoracic computer tomography (CT), among others in many different fields.

Artificial Intelligence (AI) can be applied in many different ways to fight COVID-19. As stated in [3], between the most important applications of AI in COVID-19 pandemic are: early detection of the infection from medical imaging, monitoring and prediction of the spread of the virus and mortality rates, tracing the virus by identifying hot spots, and development of drugs and vaccines by helping in clinical trials. Landing AI [4] developed a monitoring tool that issues an alert when anyone is less than the desired distance from another person, promoting social distancing in the streets due to its effectiveness to slow down the COVID-19 spread. On the other hand, machine learning methods have been applied to predict the number of active cases around the world [5], for fast COVID-19 detection from CT [6] and X-Ray [7], and to develop systems for detection of those who are not wearing facial masks [8].

Using the viral nucleic acid detection using real-time polymerase chain reaction (RT-PCR) methods for testing in thousands of suspenseful patients is very delayed. To address this drawback, efforts have been made using AI to detect patients with COVID-19 in a very fast time through medical imaging technologies like CT and X-Ray images. It is because, COVID-19 causes acute, highly lethal pneumonia with clinical symptoms similar to those reported for SARS-CoV and MERS-CoV [9]. The most common and widely available method using this type of technologies is by chest X-Ray images because it is available in ambulatory care facilities, handy with portable X-Ray systems, and enabling rapid classification (speeding up the disease screening). In contrast, CT scanners may not be available in many underdeveloped regions, disabling its use for quick diagnoses. Despite the advantages to detect COVID-19 by X-Ray, one of the main bottlenecks is the need of specialists (radiologists) to interpret the images. Taking this "specialists" expertise as *a prior* knowledge to build an AI system can help them for quick triage, especially as a tool to triage patients for radiologists with case overloads.

1.1 Related Works

Several AI-based approaches have been proposed to detect patients with COVID-19 using X-Ray images. Most of them use pre-trained models and data augmentation, mainly due to the lack of data. [7] create a free repository of X-Ray image data collections to train machine learning approaches for COVID-19 classification. In addition, [10] published a survey on public medical imaging data

resources (CT, X-Ray, MRT and others), which can be used to increase the number of X-Ray samples. Reviews of known deep learning models used to create an automatic detection of COVID-19 from X-Ray images are presented by [11] and [12], which used VGG-19, MobileNetV2, Inception, Xception and ResNetV2 as pre-trained models. They used a small number of X-Ray samples with confirmed COVID-19 (224, 50 and 25 respectively). [13] collected more X-Ray samples to increase the training dataset and use pre-trained models followed by highlighting class-discriminating regions using gradient-guided class activation maps(Grad-CAM) [14] for better visualization.

Abbas [15] introduced a model called Decompose, Transfer and Compose (DeTracC) to classify between healthy, severe acute respiratory syndrome (SARS) and COVID-19 in X-Ray images. This network was built in tree stages: (i) features extraction, (ii) class decomposition, and (iii) classification. The authors used AlexNet and ResNet18, as pre-trained models, and Principal Component Analysis (PCA), as a decomposition class. The training was performed with 80 samples of normal X-Ray, 105 samples of COVID-19, and 11 samples of SARS, and data augmentation to increase the dataset to 1764 was employed. Afshar [16] presented a new model based on capsule networks called COVIDS-CAPS to classify between non-COVID-19 (normal, Bacterial and Viral) and COVID-19 using less number of trainable parameters compared with pre-trained models. Their results show that COVIDS-CAPS is able to predict X-Ray with COVID-19. Despite the fact that the network was trained with few X-Ray samples, which poses uncertainties regarding the network suitability for new samples.

Not only AI-based research was developed (several papers using deep learning to predict COVID-19 in X-Ray images), also software and services have been created. The startup "DarwinIA" developed the COVID-Net [17], which can help to identify COVID-19 patients using chest X-Ray radiography. Also, they made a free Kubernetes Bundle for inferencing COVID-19 X-Rays images. In addition, Seoul-based medical AI software company Lunit[1] released its AI-powered software for chest X-Ray analysis with a limitation of 20 uses/day/user.

1.2 Contributions

In this context, this work presents a free and open source system available as a web service for fast detection of COVID-19 characteristics in chest X-Ray images using deep learning. This system employs deep learning models to detect COVID-19 effects on lungs from chest X-Ray, which can be used for classification, triage, and monitor COVID-19 cases.

The main contributions of this work can be summarized as follows: First, two deep learning models are presented, one to differentiate between X-Ray and non-X-Ray images based on Mobile-Net architecture, and another one to detect chest X-Ray images with characteristics of COVID-19 using a network bases on dense blocks and initialized from a pre-trained ImageNet. Second, we provide a

[1] Lunit: https://www.lunit.io/en/covid19/.

free and open-source service with dedicated GPUs to make inferences in real-time. The source code is available at https://github.com/ICA-PUC/ServiceIA-COVID-19.

The remainder of the paper is organized as follows: Sect. 2 describes the proposed methodology for the Web Service's implementation, and Sect. 3 presents the datasets employed in our experiments. Then, Sect. 4 shows the results achieved by the X-Ray images filter and COVID-19 classifier. Finally, Sect. 5 summarizes the conclusions obtained from our experiments.

2 Methodology

This section presents the methodologies adopted for each of three parts of the project, the X-Ray image filter, the COVID-19 classifier and the Web page description. Figure 1 summarizes the workflow of the system.

The first box in Fig. 1, from left to right, illustrates the beginning of the detection process. It starts with a simple extension verification to check whether the uploaded file is an image (web interface). Next, the Backend (second box) sends and stores the input image to the GPU cluster (Server), which performs the network's inferences after the Backend verifies the correct uploading of the images to it. Finally, the last box shows how the web interface stores and displays the result of the inference.

2.1 X-Ray Images Filter

Due to the input of our system to predict COVID-19 are X-Ray images from frontal AP and PA views, we first guarantee that the inputs present these characteristics to have a correct assessment. Therefore, we implement a neural network based on Mobile-Net architecture to identify whether it is a valid image (pulmonary frontal X-Ray image) or a non-valid image (rotated pulmonary X-Ray images, colored or natural images, for instance).

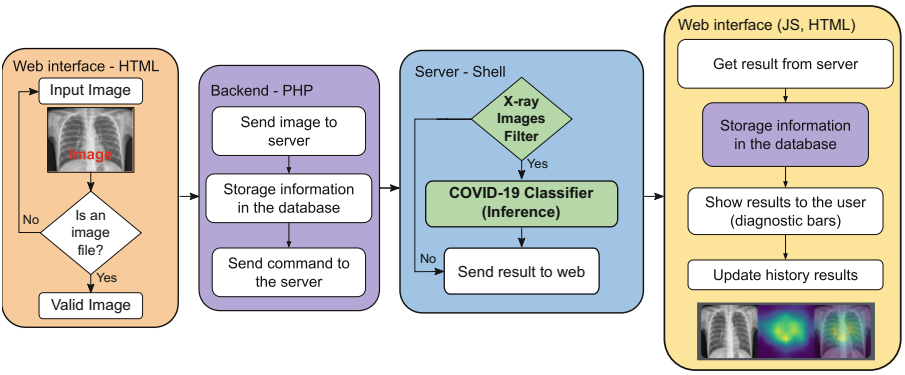

Fig. 1. Inference workflow for X-ray images. Each step refers to a single abstraction layer.

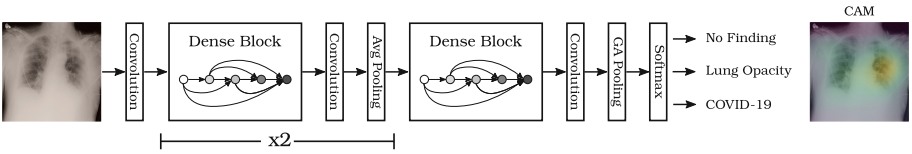

Fig. 2. Description of the neural architecture used in this work to classify X-Ray images for detection COVID-19. It is made of three DenseNet blocks, followed by a linear classifier.

2.2 COVID-19 Classifier

Figure 2 illustrates the processing scheme followed in this work to classify COVID-19 X-Ray images. The core of this system is a classifier built on the DenseNet [18] network with weights initialized from a pre-trained ImageNet [19] model. We selected a DenseNet-based architecture due to it has demonstrated high capability for classifying X-Ray images [20,21].

For optimizing the network parameters, we split this process into two stages due to the scarcity of COVID-19 samples. At the first stage, we train the DenseNet to discern between No Finding and Lung Opacity images, and at the second one, the model was finetuned incorporating the COVID-19 class information. During the first stage, COVID-19 samples were considered as Lung Opacity because of existing correlation between COVID-19 and Pneumonia, and processed independently in the second stage. By adopting this stratified training, we take advantage of the number of samples per class in the first stage to guarantee the learning of representative features for identifying opacities in the Lungs. Then, in the second stage, these features are finetuned to classify whether the opacity was originated by COVID-19 or not.

2.3 Web Page Description

The web page was created to display all the content of this research. Besides, health specialists may use the platform to support patients' classification. The web page is accessible worldwide, being available in two languages: Portuguese (original) and English. It also describes also, there is an area on the web page where public users can experience the predicted classification using personal X-Ray images. At the end of the page, it is possible to view a 3D projection based on PCA analyses, which from a set of images samples, forms groups of images that most resemble each other.

Front-End and Back-End Interface - Service Architecture: due to the web page was developed as a free service for providing a simple solution to perform image analysis, and that can be utilized by any user. The web page interface (called front-end) was developed in HyperText Markup Language (HTML), Cascading Style Sheets (CSS) and JavaScript (JS). The implemented service that maintains the operation of the website, known as backend, was developed in

Hypertext Preprocessor (PHP), Python, and Shell Command Language (Sh). The Deep Learning neural network models were implemented in Keras engine, using Tensorflow as backend. The server run over a Unix operating system, which controls the running process via Bourne-again shell (Bash).

3 X-Ray Dataset

Public data, collected from different places, was used for our implementations.

3.1 X-Ray Images Filter

For filtering frontal X-Ray images, we selected three public groups of images:

- Frontal pulmonary X-Ray [22].
- Frontal non-pulmonary X-Ray collected using Web Scraping.
- Other kind of images that are not X-Ray images: PASCAL VOC and Computational Vision at CALTECH dataset.

Taking into account that the performance of the classification system would be reduced if it process images inverted or rotated (90° clockwise and counterclockwise), we created a group of images with these characteristics to be identified as non-valid by the X-Ray filter. Particularly, we randomly selected a set of images from the X-Ray dataset and applied rotations of 90°, 180°, and 270° to each image. Table 1 summarizes the distribution of the dataset used for the filter network.

3.2 COVID-19 Classifier

For detecting COVID-19 using X-Ray imagery, we selected four publicly available datasets, two associated with COVID-19 and the others with opacities in Lungs caused by different pathologies, like pneumonia, infiltration, consolidation, among others. Both COVID-19 datasets, Cohen [7] and *Figure 1-COVID*[2] datasets, are community repositories updated regularly with X-Ray imagery from patients from different countries, already diagnosed or suspected of having COVID-19, and others pneumonia infections. At the date this paper was written, the Cohen dataset

Table 1. Dataset distribution for the X-ray images filter.

Class	Data type	# of samples			
		Train	Validation	Test	Total
Valid	Frontal pulmonary X-ray	4,400	300	300	5,000
	Rotated frontal pulmonary X-ray	4,800	100	100	5,000
Non-valid	Frontal non-pulmonary X-ray	530	100	100	730
	Not X-ray	9,800	100	100	10,000

[2] https://github.com/agchung/Figure1-COVID-chestxray-dataset.

Table 2. Distribution of samples of Chest X-Ray, RSNA, and COVID-19 datasets.

Pathology	Datasets		
	Chest X-ray	RSNA	COVID-19
No finding	1,340	8,851	–
Lung opacity	1,346	6,012	–
COVID-19	–	–	3616

contained 438 X-Ray images from AP and PA views, 359 associated with COVID-19, and 79 with the others pathologies. The *Figure 1-COVID* dataset is a smaller one comprising 40 images, where 35 are from patients confirmed with COVID-19, three with pneumonia caused by others infections, and two with no finding pathology. There is also a set of images from patients with symptoms not confirmed as positive of COVID-19 that were filtered out. We merged the Cohen and the *Figure 1-COVID* dataset forming the COVID-19 dataset.

The non-COVID-19 datasets are the Chest X-Ray Pneumonia [23] and the RSNA Pneumonia detection challenge [24]. The Chest X-Ray Pneumonia dataset contains a total of 5,863 PA view X-Ray images, collected from pediatric patients from one to five years old. The dataset is distributed into two categories: Normal or Pneumonia, and it is already organized into training, validation, and testing sets. Additionally, it also reported whether the pneumonia was caused by a virus or bacterial. From the RSNA dataset, we selected the images corresponding to the "No Finding" and "Lung Opacity" classes, filtering out the images rotated at (90°–270°) approx using the X-Ray filter. Table 2 summarizes the final distribution of samples after performed this process. In this work, we rename the images labeled as Normal and Pneumonia to the non-Finding and Lung opacity class to have the same nomenclature of RSNA dataset. Examples of the "No Finding" and "Lung Opacity" classes are shown in Fig. 3.

4 Results

This section presents the experimental protocol used to develop the networks. Afterward, it is shown and analyzed the results obtained. All experiments were carried out in an NVIDIA GPU Tesla P100 of 16 GB of RAM and 3584 Cuda cores.

4.1 X-Ray Images Filter

Experimental Protocol. The images were resized to $224 \times 224 \times 1$ and normalized between zero to one. Besides, the training samples were augmented by performing random rotations of 5° and zooming up to 10%. Table 3 summarizes the hyper-parameters setup used for training.

Result. The training time was 30 min approximately, running a total of 69 epochs, when the early-stopping was activated. The network achieved the best

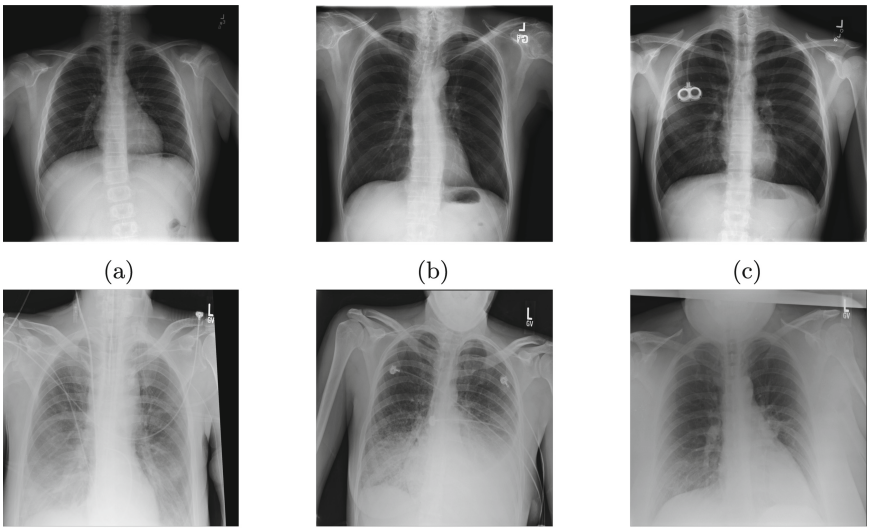

Fig. 3. Examples of images from patients labeled as no finding (a, b, c) and Lung Opacity (d, e, f).

Table 3. Training configuration used in the filter network.

Configurations	Value
Batch	128
Steps by epoch	5
Number of epochs	100 (maximum)
Optimizer	Adam
Learning rate	0.001 (decay a 0.5 factor each 5 epochs)
Stop criteria	Follow up the loss function (15)
Metrics	Accuracy

performance at epoch 54, with a loss function value of 0.0075, and 99.83% of accuracy in the validation set. Similar classification rates were obtained by evaluating the trained network in the testing set, reaching an accuracy of 99.3%.

4.2 COVID-19 Classifier

Experimental Protocol. We first split each dataset into three groups: training, validation, and testing sets, adopting different criteria for each dataset. In the COVID-19 datasets, we selected the samples according to the patient to avoid having samples from the same patient in training and validation/testing sets, respectively. Specifically, we selected a proportion of 80%, 10%, and 10% of

patients for training, validation, and testing, respectively. In the RSNA dataset, the samples were split randomly following the same proportion of the COVID-19 datasets because there is no more than one image per patient. In the Chest X-Ray Pneumonia dataset was not necessary to perform this procedure as this distribution was already provided. Finally, the corresponding groups were merged to constitute the final sets.

All images were resized to $224 \times 224 \times 3$ and normalized according to the mean and standard deviation of the ImageNet dataset. Due to the dataset imbalance, we both oversampled the COVID-19 images and weighted the cross-entropy loss to enhance the classification of COVID-19 imagery. We assigned the weights for each class using Eq. 1,

$$\omega_{c_i} = \frac{N_{c_i}}{N_{c_{max}}}, 0 < i < C \tag{1}$$

where N_{c_i} is the number of samples for class i, $N_{c_{max}}$ the majority class and C the number of classes.

Considering the presence of images potentially labeled incorrectly, it was also applied the label smoothing as a regularization technique, setting alpha to 0.1. It prevents the model from making predictions too confidently during training that can be reflected in poor generalization. Then, cross-entropy loss takes the form described in Eq. 2,

$$L = y_{soft} * \log(\hat{y}) * \omega_{c_i} + (1 - y_{soft}) * \log(1 - \hat{y}) \tag{2}$$

where $y_{soft} = (1 - \alpha) * y + \alpha/C$, and y and $\hat{y}$ the true and predicted labels, respectively.

Besides, we also augmented the training and validation samples by performing random horizontal flipping, rotation, brightness, scaling, occlusions at top of the images, cropping, and resize transformations. This procedure was carried out to avoid the network learns to maximize the inter-class differences based on the distribution of the noise that characterizes each dataset. During training, we monitored the validation loss function applying early stopping when no improvements were observed throughout five consecutive epochs. Also, the learning rate was reduced by a factor of 0.5 after a plateau on the validation loss. We initiated the learning rate of Adam optimizer to $1e{-}5$, fixing the other parameters to default values.

We assessed the performance of the model quantitatively and qualitatively. The foremost was performed in terms of Confusion Matrix, sensitivity and specificity metrics, which quantifies the classifier's ability to avoid false negatives and false positives, respectively. In particular, we report the sensitivity as diagonal of the confusion matrix. Also, the qualitative assessment was performed by analyzing the generated Class Activation Maps (CAM), which indicates the regions that were more relevant in the classification of the evaluated image.

Finally, a Visual Transformer (VIT) [25] model and four traditional machine learning techniques, Support Vector Machine (SVM), Random Forest (RF), XGBoost [26], and Multilayer Perceptron (MLP), respectively, were also evaluated and used as a baseline for our proposed methodology.

Table 4. Median and standard deviation normalized confusion matrix obtained by evaluating all classifier in the corresponding testing set after running the experiments 50 times.

		Predicted		
		No finding	Lung opacity	COVID-19
Ours	No finding	**95.80 ± 1.40%**	2.50 ± 0.80%	1.50 ± 1.20%
	Lung opacity	8.80 ± 1.70%	**90.00 ± 1.80%**	0.80 ± 0.50%
	COVID-19	1.40 ± 0.90%	0.60 ± 0.60%	**97.80 ± 1.10%**
SVM	No finding	88.22 ± 0.15%	7.53 ± 0.10%	4.25 ± 0.10%
	Lung opacity	11.73 ± 0.05%	82.80 ± 0.08%	5.47 ± 0.07%
	COVID-19	10.17 ± 0.11%	9.12 ± 0.00%	80.72 ± 0.11%
RF	No finding	89.80 ± 0.20%	11.20 ± 0.20%	6.00 ± 0.40%
	Lung opacity	14.00 ± 0.30%	78.50 ± 0.40%	4.10 ± 0.40%
	COVID-19	4.10 ± 0.20%	2.30 ± 0.20%	83.80 ± 0.50%
VIT	No finding	90.60 ± 1.30%	6.20 ± 1.10%	3.10 ± 0.60%
	Lung opacity	15.40 ± 1.40%	80.00 ± 1.60%	4.80 ± 0.90%
	COVID-19	4.70 ± 1.00%	6.60 ± 1.20%	88.70 ± 1.50%
XGBoost	No finding	91.99 ± 0.83%	2.21 ± 0.24%	5.80 ± 0.63%
	Lung opacity	1.63 ± 0.12%	82.77 ± 0.18%	15.60 ± 0.18%
	COVID-19	1.54 ± 0.05%	5.98 ± 0.22%	92.48 ± 0.27%
MLP	No finding	85.39 ± 0.59%	5.58 ± 0.35%	9.02 ± 0.59%
	Lung opacity	17.82 ± 0.84%	76.46 ± 1.02%	5.71 ± 0.55%
	COVID-19	9.66 ± 1.23%	14.91 ± 0.95%	75.41 ± 1.38%

Table 5. Results obtained by the classifier in terms of Specificity metric. It is reported the mean and standard deviations statistics as percentage (NF: No Finding, LO: Lung Opacity, C-19: COVID-19).

	SVM	RF	VIT	XGBoost	MLP	Ours
NF	88.8 ± 0.0	83.1 ± 0.3	88.1 ± 1.1	98.4 ± 0.1	92.4 ± 0.5	**93.7 ± 1.2**
LO	92.1 ± 0.1	92.8 ± 0.2	93.6 ± 1.0	95.2 ± 0.2	91.9 ± 0.4	**97.9 ± 0.6**
C-19	95.2 ± 0.1	97.9 ± 0.1	96.1 ± 0.6	87.8 ± 0.3	84.9 ± 0.8	**98.8 ± 0.9**

Results. Tables 4 and 5 summarize the performance of all assessed models in terms of the confusion matrix and specificity metrics, respectively, after executing the experiments 50 times. Specifically, we report the result in terms of the median and the standard deviation statistics for all evaluated metrics.

Results demonstrate the high capability of our method to discern between the assessed classes. In particular, it is observed that the classifier exhibits a lower rate of misclassification regarding the COVID-19 class, although the lower amount of samples. Notice the most confusion occurs between Lung Opacity and

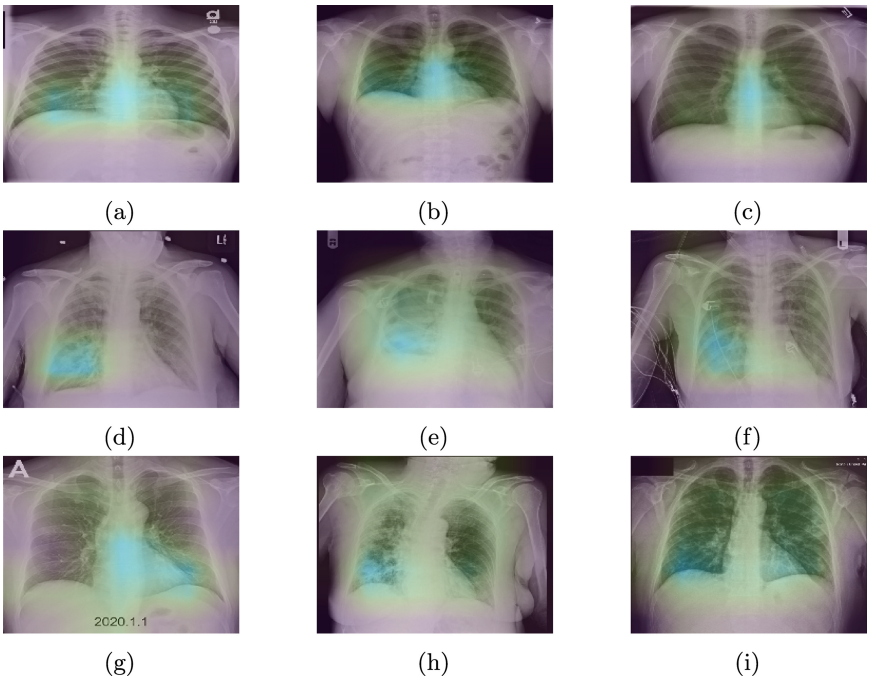

Fig. 4. Examples of images from patients labeled as non-finding (a, b, c), Lung Opacity (d, e, f), and COVID-19 (g, h, i), respectively.

No Finding samples. These results are expected considering that some of the Lung Opacity samples are very similar to the No Finding, indicating a possible early stage of the disease. These results are reflected in the specificity metric, where the classification rates are above 90.0% in median for all classes. However, it is necessary the collection of more COVID-19 images to improve the capability of the models for this task. For a real scenario, it is important to have a classifier with a lower rate of false positives to reduce the propagation of the virus, as well as with lower false positives to avoid classifying healthy persons. Additionally, it is required to have samples from different sensors to make the model more robust against particular artifacts and landmarks. Regarding the performance of other evaluated techniques, it notorious the superiority of our method in all metrics. We obtained rates above 90 for all metrics, whereas most of the others are below 90%. Interestingly, the VIT performed similarly to traditional techniques, although it has demonstrated high performance in other domains. We hypothesize that its performance was affected by the low quantity of available samples for the X-Ray domain. Among the traditional techniques, XGBoost got the higher metrics values, obtaining rates in some cases above 90%, and among all methods, it got the lowest standard deviation.

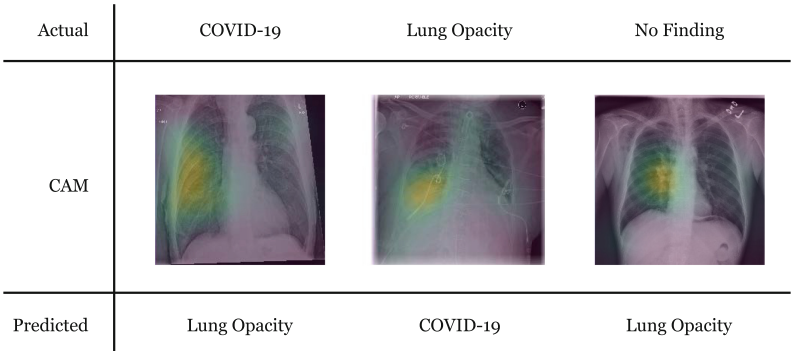

Fig. 5. Examples of images missclassified.

Figure 4 shows three examples per class of CAMs corresponding to images from the testing set. Specifically, it is shown a composition of the images and the associated CAM as heatmaps. By performing this analysis, it can be determined the most relevant regions considered by the network to make the final classification. In fact, it can be noticed the higher intensities on heatmaps are localized around the lungs as expected, and artifacts as rows or letters present on the images are ignored by the network to make the final prediction. These results suggest that the network is not making the final decision based on the noise characteristics of each dataset. In the dataset there are artifacts that can easily be identified by the network to discern between images from the assessed classes. Regarding images belonging to Lung Opacity, it is remarked that the network was able to identify the regions where these opacities occur. Similar behavior can be observed in the COVID-19 images where the network also highlights the most whited regions. These results are expected considering the high correlation between COVID-19 image and Pneumonia, as COVID-19 causes Pneumonia. For the Non Finding class, the heatmaps are concentrated in the central part of the chest, between the Lungs.

Finally, Fig. 5 shows examples of images missclassified. It can be observed that images classified as COVID-19 being of Lung Opacity, presents similar characteristics and vice-versa. This situation is expected to be common in patients with advanced degrees of pneumonia. This situation is expected to be common for patients with advanced stages of pneumonia independently the cause of it.

4.3 Web Page Interface

The site is structured in three sections, being the first one, where the user can interact with the website to test owned X-Ray images or examples available on the website. The second one describes the motivation and objectives of the project, and the third one presents the proposed solution as well as the technical explanation of its implementation.

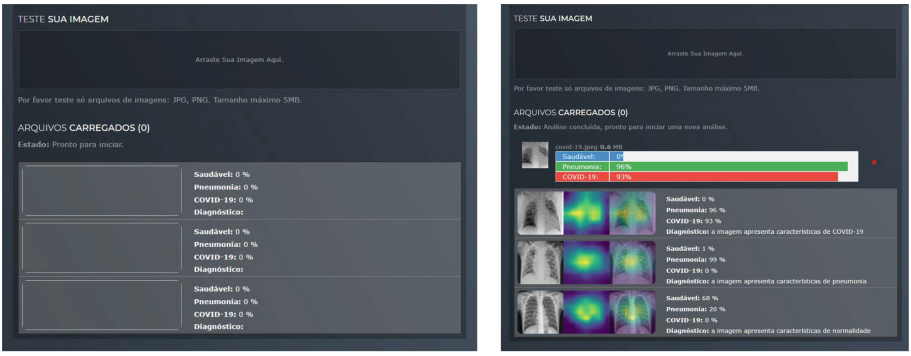

(a) (b)

Fig. 6. (a) Initial state of the site, where the user can send an X-Ray image to obtain a prediction of COVID-19. (b) Section of results: history and classification of X-Ray images tested.

Figure 6a displays a snip of the first section of the web site at its initial state, while Fig. 6b shows examples of testing performed on it. In particular, it is illustrated in diagrams of bars the result obtained for the actual test, and a history of the last experiment carried out. Besides, for each test, it is shown a brief description of the results, indicating if the image evaluated is from a healthy person, with opacity in the Lungs, or with characteristics of COVID-19.

Finally, the web page also shows an Embedding projector [27] to visualize and interpret the features extracted from 294 X-Ray images from the dataset. For instance, this projection are visualizing a basic clustering (No Finding and COVID-19 images) using the PCA algorithm.

5 Conclusion

In this work, a free web service for fast corona virus 2019 (COVID-19) classification using chest X-ray images is presented. The web service is handy and accessible, being possible to use it from desktop computer or mobile devices. It has dedicated GPUs for real-time inference and relies on two deep learning models: a model to differentiate between X-Ray and non-X-Ray images, and a model to detect COVID-19 characteristics in chest X-ray images.

The web service is composed of three main parts: a friendly web interface, an X-Ray image filter, and a COVID-19 classifier. The web interface allows the user to upload a chest X-Ray image for consultation and receive a classification, which can be Healthy, Characteristics of Pneumonia, or COVID-19. Moreover, a heatmap with the Class Activation Maps (CAM) is generated, which indicates the regions that were more relevant in the classification of the evaluated image.

An X-Ray image filter have been implemented to differentiate between valid images (pulmonary frontal X-Ray images), and non-valid images (rotated pulmonary X-Ray images, natural images, other kind of images). A pre-trained

MobileNet architecture have been employed for this purpose, achieving an accuracy of 99.3%.

The COVID-19 Classifier was implemented by optimizing a pre-trained ImageNet DenseNet. Results demonstrated the capability of the model to discern between the assessed classes, recording values above 90% in terms of sensitivity and specificity metrics. Additionally, a qualitative evaluation, based on the analysis of the generated CAM, indicates that the trained network makes its decisions focuses on the regions of the image where the Lungs are located. This analysis shows that the strategy of augmenting the data and replicating the COVID-19 samples helped to mitigate the problem of overfitting considering the scarcity of COVID-19 samples. Additionally, we evaluated the VIT, a new DL approach for image classification, and four traditional machine learning techniques. Results demonstrated that out method the highest capability for classification among all assessed methods

Future works consider the assessment of the system in hospitals to have feedback from specialists. We will provide a platform to annotate samples to increase the dataset, and retrain the network to have a more accurate model.

Besides, we will extend our methodology to make classification in Computerized Tomography images where more COVID-19 images are available.

Impact Statement

This work generates a technological impact by providing a user-friendly web service deployed using free frameworks and public datasets. It is easy to access from any device connected to the internet such as desktop computers or mobile phones. Besides, the service core is developed using Artificial Intelligence techniques to classify the X-Ray images. Moreover, this work contributes socially by helping the health sector in this time of crisis, providing a tool for decision support about COVID-19 diagnosis using X-Ray images. Furthermore, the code is open source to allow the scientific community to modify it and collaborate to improve it.

Disclaimer of Liability

It is noteworthy that there is no way to guarantee 100 % effectiveness in any predictive process. For this reason, it is extremely important that any medical diagnosis is made by specialized healthcare professionals. The objective of this project is only to assist decision-making by specialists.

Acknowledgement. This work could not have been done without the collaboration of the entire team of the Applied Computational Intelligence Laboratory (ICA) and Cenpes/Petrobras, partners for 21 years in the research and development of artificial intelligence projects for oil and gas sector.

References

1. World Health Organization Homepage. WHO Timeline - COVID-19 (2020). www.who.int/news-room/detail/27-04-2020-who-timeline--covid-19. Accessed 5th June 2020
2. World Health Organization Homepage. Coronavirus disease (COVID-19) pandemic (2020). https://www.who.int/emergencies/diseases/novel-coronavirus-2019. Accessed 22nd June 2020
3. Vaishya, R., Javaid, M., Khan, I.H., Haleem, A.: Artificial intelligence (AI) applications for COVID-19 pandemic. Diabetes Metab. Syndr. Clin. Res. Rev. **14**(4), 337–339 (2020)
4. Landing AI. Tool to help customers monitor social distancing in the workplace (2020). https://landing.ai/. Accessed 26th May 2020
5. Institute for New Economic Thinking Homepage - University of Cambridge Faculty of Economics. (INET) (2020). http://covid.econ.cam.ac.uk/linton-uk-covid-cases-predicted-peak. Accessed 27th May 2020
6. Gozes, O., et al.: Rapid AI development cycle for the coronavirus (COVID-19) pandemic: initial results for automated detection & patient monitoring using deep learning CT image analysis (2020)
7. Cohen, J.P., Morrison, P., Dao, L.: COVID-19 Image Data Collection (2020)
8. LeewayHertz. Face mask detection system (2020). https://www.leewayhertz.com/face-mask-detection-system/. Accessed 26th May 2020
9. Li, Y.-C., Bai, W.-Z., Hashikawa, T.: The neuroinvasive potential of SARS-CoV2 may play a role in the respiratory failure of COVID-19 patients. J. Med. Virol. **92**(6), 552–555 (2020)
10. Kalkreuth, R., Kaufmann, P.: COVID-19: a survey on public medical imaging data resources (2020)
11. Apostolopoulos, I.D., Mpesiana, T.A.: Covid-19: automatic detection from X-ray images utilizing transfer learning with convolutional neural networks. Phys. Eng. Sci. Med. **43**(2), 635–640 (2020). https://doi.org/10.1007/s13246-020-00865-4
12. Hemdan, E.E.-D., Shouman, M.A., Karar, M.E.: COVIDX-Net: a framework of deep learning classifiers to diagnose COVID-19 in X-ray images (2020)
13. Karim, Md.R., Döhmen, T., Rebholz-Schuhmann, D., Decker, S., Cochez, M., Beyan, O.: DeepCOVIDExplainer: explainable COVID-19 predictions based on chest X-ray images (2020)
14. Selvaraju, R.R., Cogswell, M., Das, A., Vedantam, R., Parikh, D., Batra, D.: Grad-CAM: visual explanations from deep networks via gradient-based localization. In: 2017 IEEE International Conference on Computer Vision (ICCV), pp. 618–626 (2017)
15. Abbas, A., Abdelsamea, M., Gaber, M.: Classification of COVID-19 in chest X-ray images using DeTraC deep convolutional neural network. medRxiv (2020)
16. Afshar, P., Heidarian, S., Naderkhani, F., Oikonomou, A., Plataniotis, K.N., Mohammadi, A.: COVID-CAPS: a capsule network-based framework for identification of COVID-19 cases from X-ray images. Pattern Recogn. Lett. **138**, 638–643 (2020)
17. Wang, L., Lin, Z.Q., Wong, A.: COVID-NET: a tailored deep convolutional neural network design for detection of COVID-19 cases from chest X-ray images. Sci. Rep. **10**(1), 1–12 (2020)
18. Huang, G., Liu, Z., Van Der Maaten, L., Weinberger, K.Q.: Densely connected convolutional networks. In: 2017 IEEE Conference on Computer Vision and Pattern Recognition (CVPR), pp. 2261–2269 (2017)

19. Deng, J., Dong, W., Socher, R., Li, L.-J., Li, K., Fei-Fei, L.: ImageNet: a large-scale hierarchical image database. In: 2009 IEEE Conference on Computer Vision and Pattern Recognition, pp. 248–255. IEEE (2009)
20. Gündel, S., Grbic, S., Georgescu, B., Liu, S., Maier, A., Comaniciu, D.: Learning to recognize abnormalities in chest X-rays with location-aware dense networks. In: Vera-Rodriguez, R., Fierrez, J., Morales, A. (eds.) CIARP 2018. LNCS, vol. 11401, pp. 757–765. Springer, Cham (2019). https://doi.org/10.1007/978-3-030-13469-3_88
21. Baltruschat, I.M., Nickisch, H., Grass, M., Knopp, T., Saalbach, A.: Comparison of deep learning approaches for multi-label chest X-ray classification. Sci. Rep. **9**(1), 1–10 (2019)
22. Kermany, D.S., et al.: Identifying medical diagnoses and treatable diseases by image-based deep learning. Cell **172**(5), 1122–1131 (2018)
23. Kermany, D., Zhang, K., Goldbaum, M.: Labeled Optical Coherence Tomography (OCT) and Chest X-Ray Images for Classification (2018). Mendeley Data, v2, https://doi.org/10.17632/rscbjbr9sj, https://nihcc.app.box.com/v/ChestXray-NIHCC
24. Wang, X., Peng, Y., Lu, L., Lu, Z., Bagheri, M., Summers, R.M.: ChestX-ray8: hospital-scale chest X-ray database and benchmarks on weakly-supervised classification and localization of common thorax diseases. In: Proceedings of the IEEE conference on Computer Vision and Pattern Recognition, pp. 2097–2106 (2017)
25. Dosovitskiy, A., et al.: An image is worth 16x16 words: transformers for image recognition at scale. ICLR (2021)
26. Chen, T., Guestrin, C.: XGBoost: a scalable tree boosting system. CoRR, abs/1603.02754 (2016)
27. Smilkov, D., Thorat, N., Nicholson, C., Reif, E., Viégas, F.B., Wattenberg, M.: Embedding projector: interactive visualization and interpretation of embeddings. arXiv preprint arXiv:1611.05469 (2016)